Supplementary Information

High-Performance, Ambient-Processable Organic Solar Cells Achieved by Single Terpene-Based Entirely Eco-Friendly Process

Hyerin Jeon[a], Jin-Woo Lee[a], Kihyun Bae[a], Tan Ngoc-Lan Phan[a], Chulhee Lim[a], Jaeyoung Choi[a], Cheng Wang[b], Seungjin Lee[c,], and Bumjoon J. Kim[a,]**

[a] Department of Chemical and Biomolecular Engineering, Korea Advanced Institute of Science and Technology (KAIST), Daejeon 34141, Republic of Korea

[b] Advanced Light Source, Lawrence Berkeley National Laboratory, 1 Cyclotron Road, Berkeley, CA 94720, United States

[c] Photoenergy Research Center, Korea Research Institute of Chemical Technology (KRICT), Daejeon 34114, Republic of Korea

* All correspondence should be addressed to B. J. K. and S. Lee (E-mail: bumjoonkim@kaist.ac.kr, 332sjin@krict.re.kr)

Supplementary Schemes, Figures, and Tables

Scheme S1. Synthetic scheme for MYBO.

Fig. S1. ^{1}H NMR spectrum of BTP-BO-2CHO in methylene chloride-d_2.

Fig. S2. ^{1}H NMR spectrum of MYBO in chloroform-d_2.

Fig. S3. MALDI-ToF spectrum of MYBO.

Fig. S4. CVs of (a) PTQ10 donor, (b) L8-BO, (c) MYBO, and (d) ferrocene. (e) Energy levels of PTQ10 and SMAs.

Fig. S5. Photograph of SMA solutions dissolved in Eu (5 mg mL^{-1}).

Fig. S6. UV–Vis absorption spectra of (a) pristine PTQ10, L8-BO, and MYBO, and (b) L8-BO and MYBO blend with PTQ10 in film state.

Fig. S7. UV–Vis absorption spectra of pristine solution (a) L8-BO, and (b) MYBO in toluene at different temperatures.

Fig. S8. DSC thermograms of pristine SMA films with different processing solvents obtained during the 1st heating cycle.

Fig. S9. Summary of PCEs of terpene-based OSCs depending on the total LD50 value from the literature and this work. Total LD50 was calculated by summation of the ATE value.

Fig. S10. Light intensity-dependent J_{SC} plots of PTQ10-based OSCs.

Fig. S11. Orientation of crystalline domains in (a) L8-BO, and (b) MYBO-based blends processed from Eu.

Fig. S12. DSC thermograms of blend films with different processing solvents obtained during the 1st heating cycle.

Fig. S13. (a) 2D contour maps of *in-situ* UV–Vis absorption spectra of PTQ10:SMA systems processed with CF and their (b) changes in absorbance at the λ_{max} of PTQ10 and SMA.

Table S1. Molecular weight information of PTQ10 donor measured by GPC at 80°C using *ortho*-dichlorobenzene as eluent.

Table S2. Calculation of HSPs of PTQ10 with functional group contribution terms.

Table S3. Calculation of HSPs of L8-BO with functional group contribution terms.

Table S4. Calculation of HSPs of MYBO with functional group contribution terms.

Table S5. Optical properties of pristine SMA films with toluene (Tol) and Eu.

Table S6. DSC results and SCLC electron mobilities of the pristine SMA films.

Experimental Section

Materials: All solvents were purchased from Tokyo Chemical Industry Co., LTD and Thermo Fisher Scientific Inc. Poly[(thiophene)-*alt*-(6,7-difluoro-2-(2-hexyldecyloxy)quinoxaline)] (PTQ10) was synthesized by previous study procedures.[1] 2,2'-((2*Z*,2'*Z*)-((12,13-bis(2-ethylhexyl)-3,9-(2-butyloctyl)-12,13-dihydro-[1,2,5]thiadiazolo[3,4-*e*]thieno[2",3'':4',5']thieno[2',3':4,5]pyrrolo[3,2-*g*]thieno[2',3':4,5]thieno[3,2-*b*]indole-2,10-diyl)bis(methanylylidene))bis(5,6-difluoro-3-oxo-2,3-dihydro-1*H*-indene-2,1-diylidene))dimalononitrile (L8-BO) was purchased from Solarmer Inc. 3,9-bis(2-butyloctyl)-12,13-bis(2-octyldodecyl)-12,13-dihydro-[1,2,5]thiadiazolo[3,4-*e*]thieno[2",3":4',5']thieno[2',3':4,5]pyrrolo[3,2-*g*]thieno[2',3':4,5]thieno[3,2-*b*]indole (BTP-BO) for the synthesis of MYBO was purchased from Derthon Opto electronic Materials Sci. Tech. Co., Ltd. Poly[(9,9-bis(3′-((*N*,*N*-dimethyl)-*N*-ethylammonium)propyl)-2,7-fluorene)-*alt*-5,5′-bis(2,2′-thiophene)-2,6-naphthalene-1,4,5,8-tetracaboxylic-*N*,*N*′-di(2-ethylhexyl)imide]dibromide (PNDIT-F3N-Br) was synthesized according to the reported method.[2]

Synthesis of MYBO

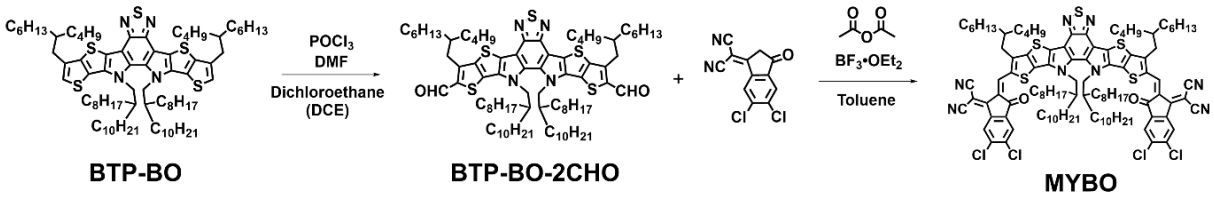

Scheme S1. Synthetic scheme for MYBO.

(1) ***Synthesis of 3,9-bis(2-butyloctyl)-12,13-bis(2-octyldodecyl)-12,13-dihydro-[1,2,5]thiadiazolo[3,4-e]thieno[2'',3'':4',5']thieno[2',3':4,5]pyrrolo[3,2-g]thieno[2',3':4,5]thieno[3,2-b]indole-2,10-dicarbaldehyde (BTP-BO-2CHO)***

0.20 g of BTP-BO (1.0 equiv.) was placed in a 20 mL microwave vial. The vial was subjected to vacuum conditions and subsequently purged with argon gas three times. 5 mL of dichloroethane was then added to fully dissolve the reactant. Following this, 0.14 mL of phosphorus oxychloride ($POCl_3$; 10.0 equiv.) and 0.46 mL of *N*,*N*-dimethylformamide (DMF; 40.0 equiv.) were introduced into the solution. The resultant mixture was stirred vigorously for 12 hr at 60°C. After the reaction, the crude product was washed with water and extracted three times using dichloromethane. The residual solvent was removed using a rotary evaporator, and the crude material was purified by column chromatography, utilizing hexane and dichloromethane as eluents. The purified product was obtained as an orange liquid (0.20 g, yield: 96%).

^{1}H NMR (400 MHz, methylene chloride-d_2) δ 10.16 (s, 2H), 4.69 (d, J = 7.8 Hz, 4H), 3.16 (d, J = 7.4 Hz, 4H), 2.10 (s, 4H), 1.54–1.15 (m, 55H), 1.13–0.71 (m, 71H).

(2) ***Synthesis of 2,2'-((2Z,2'Z)-((3,9-bis(2-butyloctyl)-12,13-bis(2-octyldodecyl)-12,13-dihydro-[1,2,5]thiadiazolo[3,4-e]thieno[2'',3'':4',5']thieno[2',3':4,5]pyrrolo[3,2-g]thieno[2',3':4,5]***

thieno[3,2-b]indole-2,10-diyl)bis(methaneylylidene))bis(5,6-dichloro-3-oxo-2,3-dihydro-1H-indene-2,1-diylidene))dimalononitrile (MYBO)

0.20 g of BTP-BO-2CHO (1.0 equiv.) and 0.08 g of IC-2Cl (2.1 equiv.) were placed in a 20 mL microwave vial. The vial was evacuated under vacuum and then purged with argon gas three times. 10 mL of toluene was added to fully dissolve the reactants. Subsequently, 0.020 mL of boron trifluoride diethyl etherate (BF_3•OEt_2; 1.0 equiv.) and 0.014 mL of acetic anhydride (4.0 equiv.) were introduced into the solution. The resulting mixture was stirred vigorously for 2 hr at room temperature. After the reaction, the crude product was precipitated in 100 mL of methanol and filtered using filter paper. Then, the residual methanol in the filtered material was fully removed by vacuum. The crude materials were purified by column chromatography with hexane and chloroform as eluents. The purified product was obtained as a black solid (0.21 g, yield: 78%).

^{1}H NMR (400 MHz, chloroform-*d*) δ 9.21 (s, 2H), 8.84 (s, 2H), 7.99 (s, 2H), 4.78 (d, *J* = 7.8 Hz, 4H), 3.22 (d, *J* = 7.6 Hz, 4H), 2.12 (s, 4H), 1.56–1.10 (m, 65H), 1.02 (d, *J* = 14.9 Hz, 33H), 0.85 (ddt, *J* = 17.0, 14.4, 7.1 Hz, 28H).

Calculated molar mass for MYBO ($M_{calcd.}$) was 1882.45 g mol^{-1} and estimated molar mass with MALDI-ToF ($M_{MALDI\text{-}ToF}$) was 1882.39 g mol^{-1}.

Characterizations: Bruker AVANCE NEO (9.4 T)-400 MHz spectrometer was used to obtain the proton nuclear magnetic resonance (^{1}H NMR) spectra of the materials, and the chemical shifts in the spectra have units of ppm. Matrix-assisted laser desorption/ionization time of flight (MALDI-ToF) spectra was measured by Autoflex maX from Bruker. The number-average molecular weight (M_n) and dispersity ($Đ$) of the polymer donor PTQ10 was measured using gel permeation chromatography (GPC) at 80°C using *ortho*-dichlorobenzene as an eluent, which was calibrated using polystyrene standard. The optimized molecular structures and the relaxed potential surface energy from bond rotation were computed using the density functional theory (DFT) method with the Becke three-parameter Lee-Yang-Parr (B3LYP) function and the 6-31G* basis set via a modeling software (Guassian 09).

Cyclic voltammetry (CV) was performed using a EG and G Parc model 273 Å potentiostat/galvanostat system in a 0.1 M tetrabutylammonium perchlorate solution with nitrogen degassed anhydrous acetonitrile as the supporting electrolyte, at a scan rate of 50 mV s^{-1}. A glassy carbon electrode was used as the working electrode. A platinum wire was used as the counter electrode, and an Ag/AgCl electrode was used as the reference electrode. The redox couple ferricenium/ferrocene was used as external standard. HOMO and LUMO energy levels were estimated from cyclic voltammetry: E_{HOMO} (eV) = $-(E_{onset}^{ox.} - E_{onset}^{Fc/Fc+}) + E_{HOMO}^{Fc}$; E_{LUMO} (eV) = $-(E_{onset}^{red.} - E_{onset}^{Fc/Fc+}) + E_{HOMO}^{Fc}$; $E_{onset}^{Fc/Fc+}$= 0.44 eV, E_{HOMO}^{Fc}= −4.8 eV.

To determine the solubility, 10 μL of eucalyptol (Eu) was incrementally added to a vial containing 3 mg of small molecule acceptors (SMAs) at room temperature.[3] The mixture was then heated to 100 ℃ for 30 min. This procedure was repeated until the SMAs were completely dissolved, with no particles remaining in the solutions. The point at which this occured was identified as the solubility threshold.

A UV-1800 spectrophotometer was used for the ultraviolet-visible (UV–Vis) absorption spectra. *In-situ* UV–Vis absorption spectra were obtained at intervals of every 0.05 s using an

HRR2000+CG spectrometer equipped with a DH-2000-BAL balanced deuterium tungsten light source. The OceanView spectroscopy software was utilized for conducting the meausrements. The differential scanning calorimetry (DSC) profiles were recorded by TA Instruments DSC 25 with heating and cooling rates of 5 ℃ min^{-1} from 20 to 330℃ for L8-BO, while the DSC thermogram of MYBO was measured in the range of 20 to 270℃. The atomic force microscopy (AFM) images were measured by NX10 from Park Systems.

The resonant soft X-ray scattering (RSoXS) experiment was performed at beamline 11.0.1.2 in the S11 Advanced Light Source (United States). Blend films for the RSoXS measurement were prepared on a 100 nm-thick, 1.0 mm × 1.0 mm Si_3N_4 membrane supported by a 200-μm thick, 5 mm × 5 mm silicon frame (Norcada Inc.). The domain size of a blend film was approximated to be half of the domain spacing (domain spacing= $2\pi q_{peak}^{-1}$) from the RSoXS profile. The relative domain purity was estimated as the relative ratio of square-root of the integrated scattering intensity in the Iq^2 vs. q plot. Grazing incidence wide-angle X-ray scattering (GIWAXS) measurements were conducted at the Pohang Accelerator Laboratory (beamline 3C, Republic of Korea), with incidence angles between 0.12 – 0.14°. Correlation length (L_c) values of the crystallites were calculated using the Scherrer equation:

$$L_c = \frac{2\pi K}{\Delta q}$$

(K (shape factor) = 0.9 and Δq = full width half maximum (FWHM) of the scatterings)

The relative degree of crystallinity (rDoC) and the information of packing orientation were determined from the pole figure of (010) π–π stacking peak, which was background-subtracted and normalized by sample volume and X-ray irradiation time. rDoC values were calculated from the following equation:

$$\text{rDoC} \propto \int_0^{\frac{\pi}{2}} I(w) \sin(w)\, dw$$

where ω is the polar angle, $I(w)$ is the scattering, and $\sin(w)$ is the geometrical correction factor.

Space-charge limited current (SCLC) mobility measurements: The hole mobilities (μ_h) for blend films and the electron mobilities (μ_e) of the neat SMA films and blend films were estimated from the SCLC method. For measuring μ_h values of devices, the device structure was ITO/ poly(3,4-ethylenedioxythiophene):poly(styrenesulfonate) (PEDOT:PSS)/active layer/Au. For measuring μ_e values of devices, the device configuration of ITO/ZnO/active layer or pristine SMA/poly[9,9-bis(3′-(*N*,*N*-dimethyl)-*N*-ethylammoinium-propyl-2,7-fluorene)-*alt*-2,7-(9,9-dioctylfluorene)]dibromide (PFN-Br)/Al was used. The preparation for active layers followed the same conditions as those described for the OSC fabrications. The current-voltage measurements were conducted with the applied voltage range of 0 to 6 V, and the obtained results were fitted using the Mott-Gurney law.

$$J = \frac{9\varepsilon_r \varepsilon_0 \mu V^2}{8L^3}$$

where J denotes the current density, ε_r represents the relative dielectric constant of the films, ε_0 exhibits the permittivity of free space (8.85×10^{-14} F cm^{-1}), μ is the charge carrier (hole or electron) mobility, V is the calculated potential across the SCLC device ($V = V_{applied} - V_{bi} - V_r$, where V_{bi} is the built-in state potential and V_r is the voltage drop resulting from resistance), and L is the thickness of the blend or pristine films measured by AFM.

Summation of LD50 in terpene mixture: To estimate the total LD50 from terpene mixture (co-solvent, solvent additive, etc.), the acute toxicity estimate (ATE) of mixture was calculated using the following equation:

$$\frac{100}{\mathrm{ATE_{mix}}} = \sum_n \frac{\mathrm{C_i}}{\mathrm{ATE_i}}$$

where ATE_{mix} is the total LD50 for mixture, C_i is the concentration of solvent i, n is the number of solvents, and ATE*i* is the LD50 of solvent.[4]

Organic Solar Cell (OSC) Fabrication and Characterization: The OSCs with a conventional architecture of indium tin oxide (ITO)/PEDOT:PSS/active layer/PNDIT-F3N-Br/Ag were prepared with the following procedures. ITO-coated glass substrates were treated by ultrasonication with acetone, deionized water, and isopropyl alcohol. Then, the ITO substrates were dried for 6 hr in an oven (70°C) at an ambient pressure, and then plasma treated for 10 min. Spin-coating of the PEDOT:PSS solution (Clevios, AI4083) was performed at 3500 rpm for 30 s onto the ITO substrates. Then, the film/substrate was annealed in the air at 160°C for 15 min before transferring into an N_2–filled glovebox. The active layer solution for the PTQ10:SMA blend system consisting the 1:1.2 weight ratio of donor to acceptor was prepared as 16.0 mg mL^{-1} concentration in chloroform (CF) without additive spin-coated onto the PEDOT:PSS/ITO substrate at 50℃ to form an active layer with a thickness of ~110 nm. Processed from Eu, the active layer solutions were prepared as 30.0 mg mL^{-1} concentration with the condtion of spin-coating at 4000 rpm for 80 s at 100℃. Then, the samples were dried with high vacuum ($<10^{-6}$ torr) for 1 hr and annealed at 100℃ for 10 min. PNDIT-F3N-Br in methanol (1 mg mL^{-1}) was then spin-coated with the condition of 3000 rpm for 30 s. Finally, Ag (120 nm) was deposited under high vacuum ($<10^{-6}$ Torr) in an evaporation chamber. For testing the air-stability of OSC fabricated under ambient condition, the OSCs with an inverted configuration (ITO/zinc oxide (ZnO)/active layer/MoO_3/Ag) were prepared. The first procedure is plasma treatment for 10 min, then the ITO substrate was spin coated with ZnO at 4000 rpm for 30 s. The ZnO-coated ITO was thermally annealed at 215℃ for 10 min. The active layer solution is same with normal type of OSCs, and for hole transporting layer, MoO_3 (10 nm) was deposited on the active layer/substrate. Lastly, Ag (120 nm) was deposited using

the evaporation chamber under the high vacuum conditions. Optical microscopy (OM) was used to measure the exact photoactive area of the mask (0.04 cm^2). Keithley 2400 SMU instrument was used to measure the PCE values under an Air Mass 1.5 G solar simulator (100 mW cm^{-2}, solar simulator: K201 LAB55, McScience), satisfying the Class AAA, ASTM Standards. K801SK302 of McScience was used as a standard silicon reference cell to calibrate the exact solar intensity. The reference cell was calibrated every 3 months, and the most recent calibration date was August 19, 2024. K3100 IQX, McScience Inc. instrument was used to analyze the EQE spectra, equipped with a monochromator (Newport) and an optical chopper (MC 2000 Thorlabs).

Air stability test of the OSCs: To measure air stability, the OSCs were fabricated in air and stored under ambient and dark conditions without encapsulation. The OSCs, which had a complete device structure (ITO/ZnO/active layer/MoO_3/Ag) and were not encapsulated, were measured with the same instrument and method as described above.

Supplementary Figures & Tables

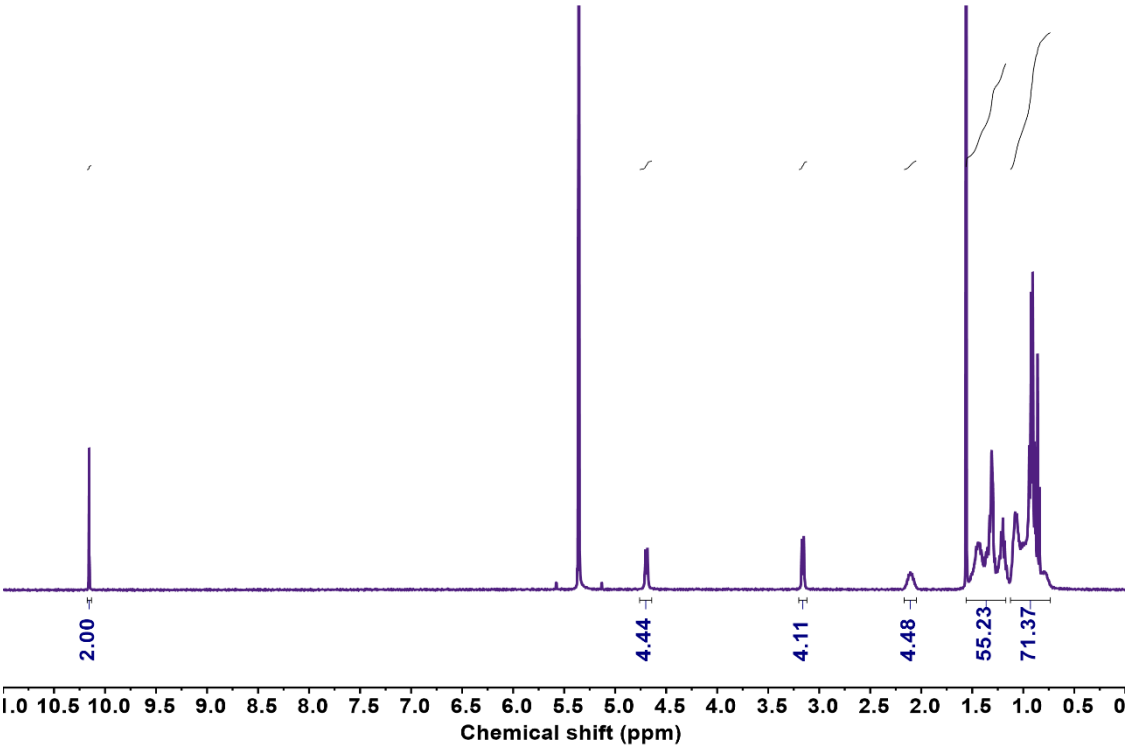

Fig. S1. ^{1}H NMR spectrum of BTP-BO-2CHO in methylene chloride-d_2.

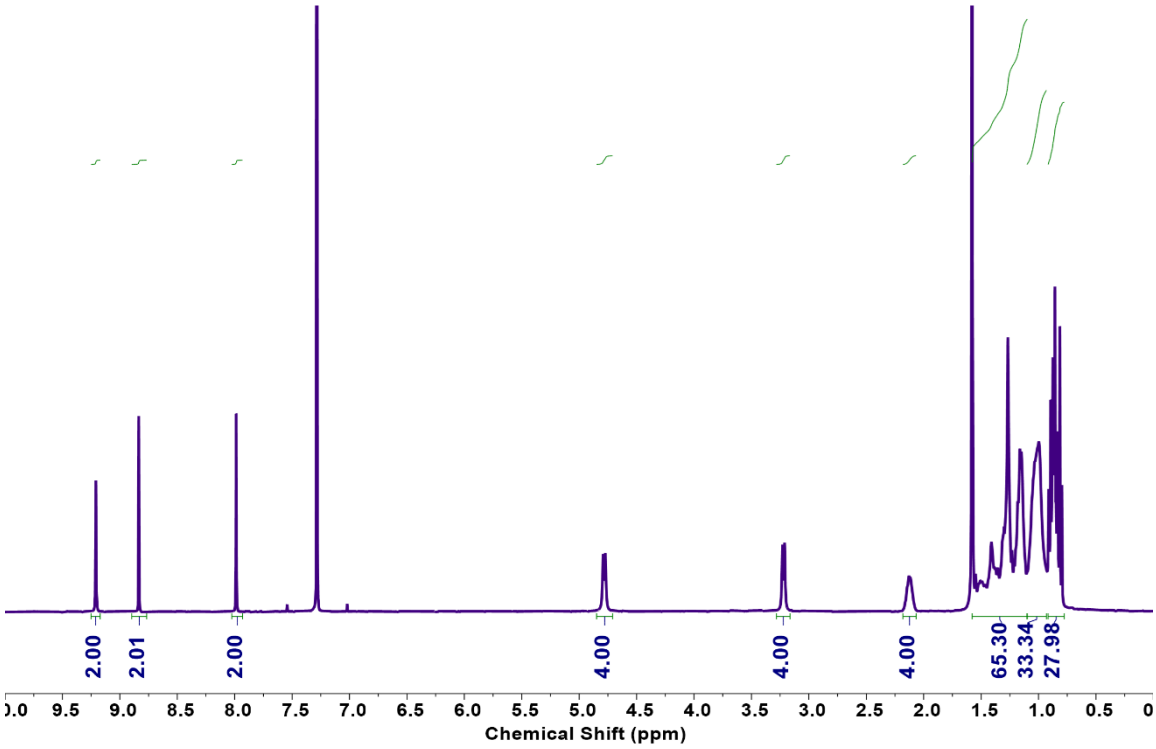

Fig. S2. ^{1}H NMR spectrum of MYBO in chloroform-d_2.

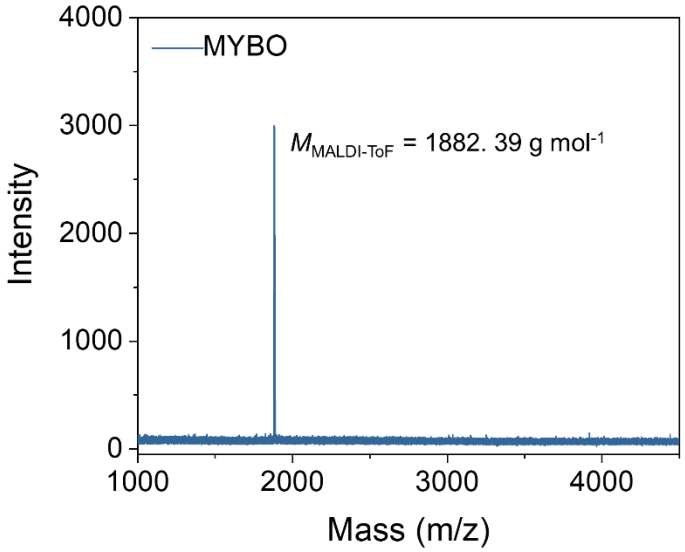

Fig. S3. MALDI-ToF spectrum of MYBO.

Table S1. Molecular weight information of PTQ10 donor measured by GPC at 80°C using *ortho*-dichlorobenzene as eluent.

Polymer	M_n **[kg mol^{-1}]**	$Đ$
PTQ10	33.2	3.5
	26.3	3.8
	20.6	3.6

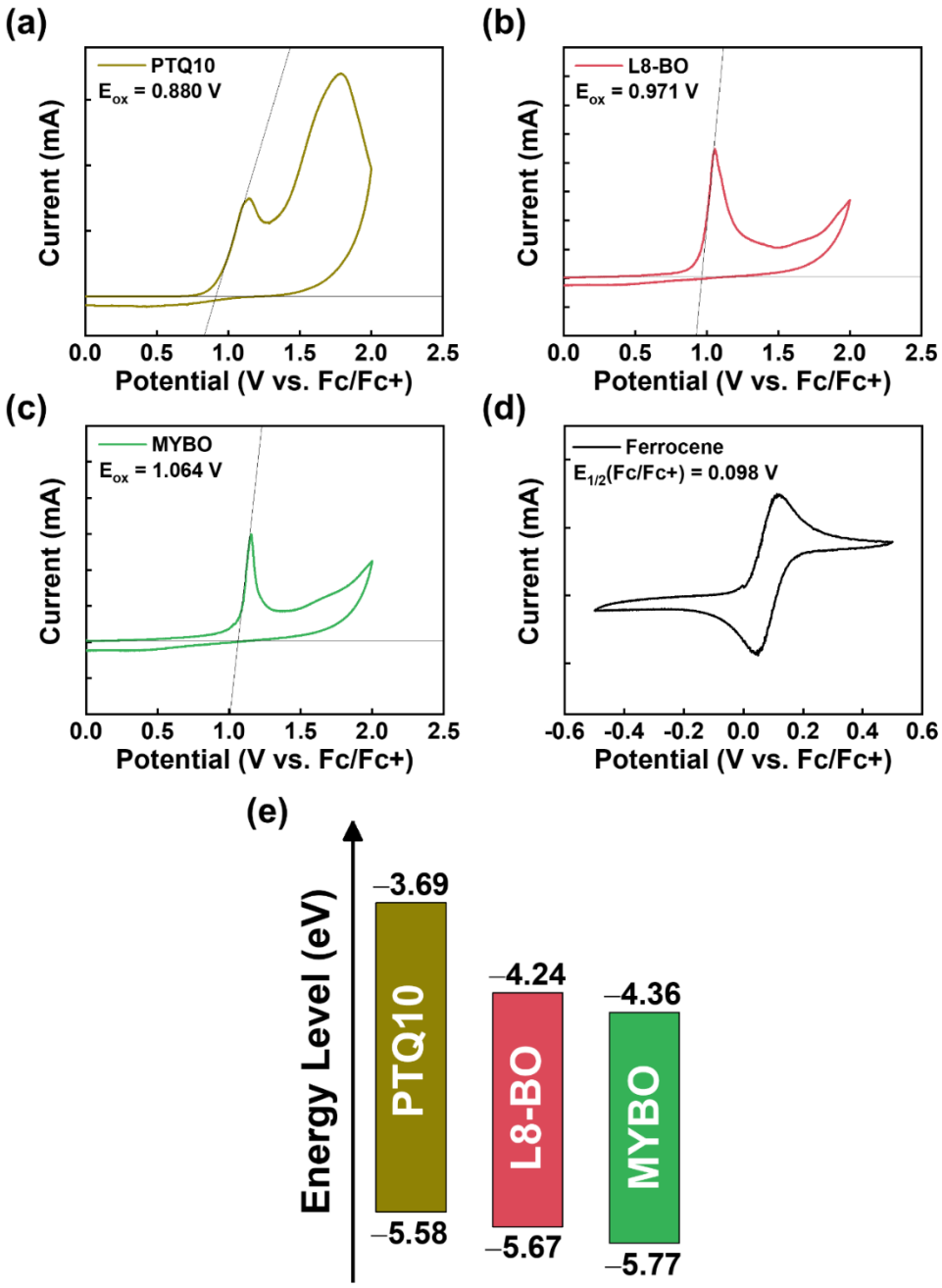

Fig. S4. CVs of (a) PTQ10 donor, (b) L8-BO, (c) MYBO, and (d) ferrocene. (e) Energy levels of PTQ10 and SMAs.

Table S2. Calculation of HSPs of PTQ10 with functional group contribution terms.

Functional Group	**Occurence**	$\sum V$ **[cm^3 mol^{-1}]**	$\sum F_{di}$ **[J$^{1/2}$ cm$^{3/2}$ mol^{-1}]**	$\sum F_{pi}$ **[J$^{1/2}$ cm$^{3/2}$ mol^{-1}]**	$\sum U_{hi}$ **[J mol^{-1}]**
-S-	1	8	454	362	221
-F	2	36	442	1084	0
=N-	2	8	328	2646	3518
-O-	1	3.8	100	401	1467
-CH_3	2	63.4	838	0	0
-CH_2-	13	215.8	3510	0	0
>CH-	1	-1	80	0	0
>C=	9	-51.3	405	630	1287
=CH-	3	37.2	669	210	429
Total		319.9	6826	5333	6922

From the calculation above δ_D, δ_P, and δ_H values were estimated to be 21.34 MPa$^{1/2}$, 0.23 MPa$^{1/2}$, 4.65 MPa$^{1/2}$, respectively, with Hoftyzer and van Krevelen method.[5]

Table S3. Calculation of HSPs of L8-BO with functional group contribution terms.

Functional Group	**Occurence**	$\sum V$ **[cm^3 mol^{-1}]**	$\sum F_{di}$ **[J$^{1/2}$ cm$^{3/2}$ mol^{-1}]**	$\sum F_{pi}$ **[J$^{1/2}$ cm$^{3/2}$ mol^{-1}]**	$\sum U_{hi}$ **[J mol^{-1}]**
-S-	5	40	2270	1810	1105
-CO-	2	20	582	1538	1956
-F	4	72	884	2168	0
-CN	4	89.6	1720	4404	4884
>N-	2	-18	62	298	732
=N-	2	8	328	2646	3518
-CH_3	8	253.6	3352	0	0
-CH_2-	28	464.8	7560	0	0
>CH-	4	-4	320	0	0
>C=	32	-182.4	1440	2240	4576
=CH-	6	74.4	1338	420	858
Total		818	19856	15524	17629

From the calculation above δ_D, δ_P, and δ_H values were estimated to be 24.27 MPa$^{1/2}$, 0.15 MPa$^{1/2}$, 4.64 MPa$^{1/2}$, respectively, with Hoftyzer and van Krevelen method.[5]

Table S4. Calculation of HSPs of MYBO with functional group contribution terms.

Functional Group	Occurence	$\sum V$ [$cm^3\ mol^{-1}$]	$\sum F_{di}$ [$J^{1/2}\ cm^{3/2}\ mol^{-1}$]	$\sum F_{pi}$ [$J^{1/2}\ cm^{3/2}\ mol^{-1}$]	$\sum U_{hi}$ [$J\ mol^{-1}$]
-S-		40	2270	1810	1105
-CO-	2	20	582	1538	1956
-Cl		101.2	1676	2456	820
-CN	4	89.6	1720	4404	4884
>N-	2	-18	62	298	732
=N-	2	8	328	2646	3518
$-CH_3$	8	253.6	3352	0	0
$-CH_2-$	52	863.2	14040	0	0
>CH-	4	-4	320	0	0
>C=	32	-182.4	1440	2240	4576
=CH-	6	74.4	1338	420	858
Total		1245.6	27128	15812	18449

From the calculation above δ_D, δ_P, and δ_H values were estimated to be 21.78 $MPa^{1/2}$, 0.10 $MPa^{1/2}$, 3.85 $MPa^{1/2}$, respectively, with Hoftyzer and van Krevelen method.[5]

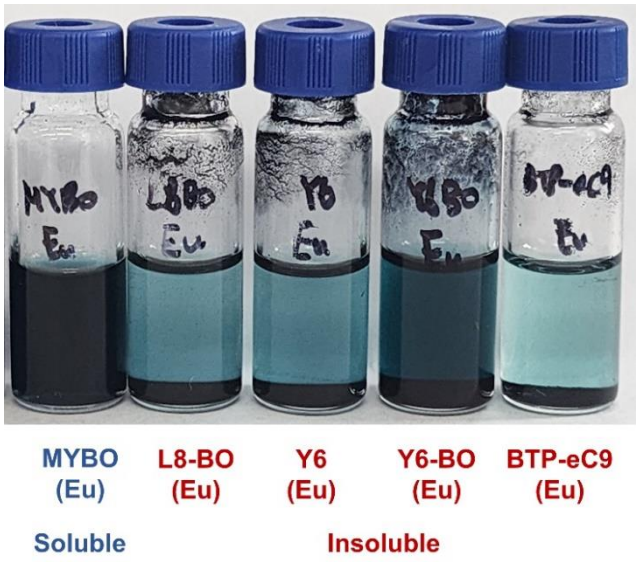

Fig. S5. Photograph of SMA solutions dissolved in Eu (5 mg mL^{-1}).

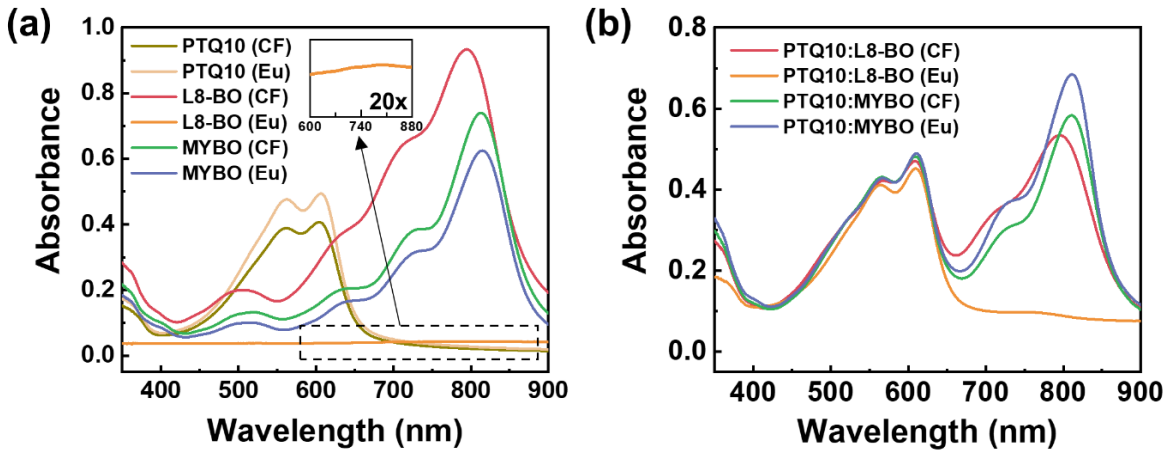

Fig. S6. UV–Vis absorption spectra of (a) pristine PTQ10, L8-BO, and MYBO, and (b) L8-BO and MYBO blend with PTQ10 in film state.

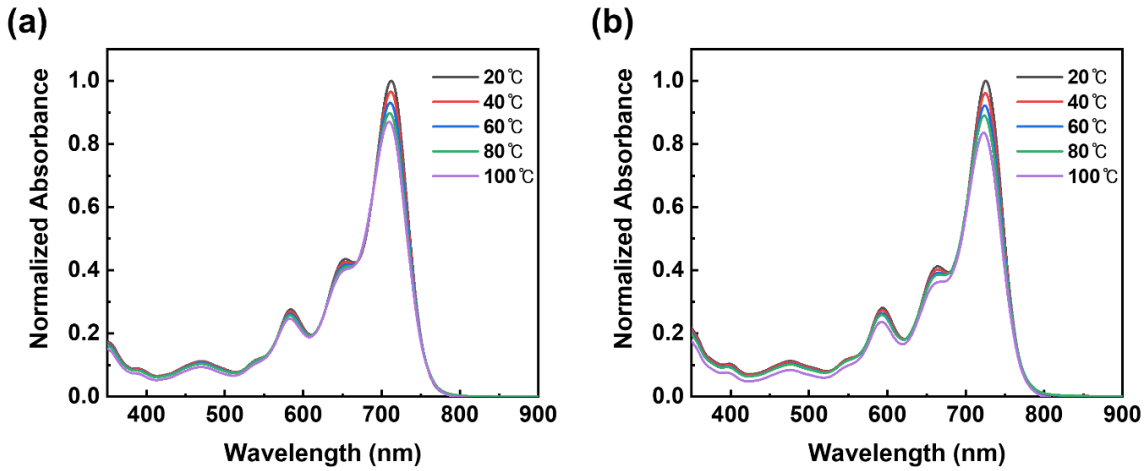

Fig. S7. UV–Vis absorption spectra of pristine solution (a) L8-BO, and (b) MYBO in toluene at different temperatures.

Table S5. Optical properties of pristine SMA films with toluene (Tol) and Eu.

Material	$I_{max}^{100°C}/I_{max}^{20°C}$
L8-BO (Tol)	0.87
L8-BO (Eu)	1.82
MYBO (Tol)	0.84
MYBO (Eu)	0.91

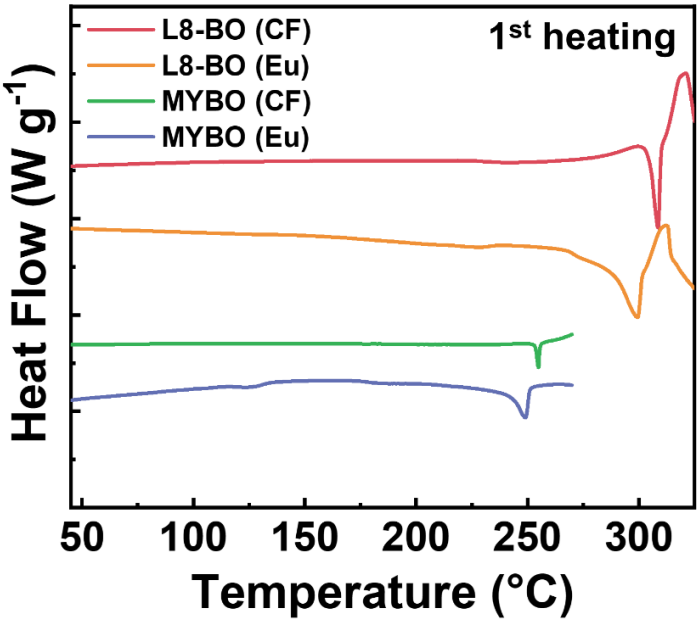

Fig. S8. DSC thermograms of pristine SMA films with different processing solvents obtained during the 1st heating cycle.

Table S6. DSC results and SCLC electron mobilities of the pristine SMA films.

SMA	T_m [°C]	ΔH_m [J g^{-1}]	μ_e[a] [cm^2 V^{-1} s^{-1}]
L8-BO (CF)	309	35.1	1.7×10^{-4}
L8-BO (Eu)	299	51.2	8.8×10^{-7}
MYBO (CF)	255	8.1	1.2×10^{-4}
MYBO (Eu)	249	18.9	1.1×10^{-4}

[a]Average values obtained from at least 3 independent devices.

Table S7. Photovoltaic performances of PTQ10:L8-BO-based OSCs processed from CF with different solution temperature and thickness.

Solution Temperature [°C]	Spin-coating Speed [rpm]	V_{OC} [V]	J_{SC} [mA cm^{-2}]	FF	PCE_{max} (PCE_{avg}) [%]
20	3000	0.90	24.35	0.62	13.58 (13.09)
35	3000	0.91	24.39	0.63	13.94 (13.70)
50	3000	0.91	24.64	0.64	14.45 (14.16)
50	4500	0.93	24.06	0.67	15.04 (14.74)

Table S8. Photovoltaic performances of PTQ10:MYBO-based OSCs processed from CF with different solution temperature.

Solution Temperature [°C]	V_{OC} [V]	J_{SC} [mA cm^{-2}]	FF	PCE_{max} (PCE_{avg}) [%]
20	0.88	24.22	0.59	12.59 (12.22)
35	0.90	24.81	0.61	13.52 (13.26)
50	0.90	23.62	0.67	14.34 (13.81)

Table S9. Photovoltaic performances of PTQ10:MYBO-based OSCs processed from CF with different thickness.

Concentration [mg mL^{-1}]	Spin-coating Speed [rpm]	V_{OC} [V]	J_{SC} [mA cm^{-2}]	FF	PCE_{max} (PCE_{avg}) [%]	Thickness [nm]
16	1200	0.89	24.67	0.51	11.13 (10.71)	155 ± 4
	2000	0.90	24.76	0.62	13.71 (13.51)	123 ± 3
	3000	0.91	24.91	0.65	14.84 (14.81)	111 ± 4
	4500	0.90	23.22	0.63	13.27 (12.82)	77 ± 4

Table S10. Photovoltaic performances of PTQ10:MYBO-based OSCs processed from Eu with different solution temperature.

Solution Temperature [°C]	V_{OC} [V]	J_{SC} [mA cm^{-2}]	FF	PCE_{max} (PCE_{avg}) [%]
20	0.82	20.28	0.46	7.59 (6.74)
40	0.83	20.70	0.53	8.99 (7.62)
60	0.88	21.57	0.59	11.20 (10.35)
80	0.87	21.70	0.65	12.21 (11.77)
100	0.88	23.15	0.64	13.11 (12.56)
120	0.88	22.56	0.61	12.12 (12.00)
140	0.88	21.09	0.65	12.03 (11.49)

Table S11. Photovoltaic performances of PTQ10:MYBO-based OSCs processed from Eu with different molecular weight of PTQ10.

PTQ10 M_n [kg mol^{-1}]	V_{OC} [V]	J_{SC} [mA cm^{-2}]	FF	PCE_{max} (PCE_{avg}) [%]
21	0.89	23.10	0.61	12.54 (12.09)
26	0.88	23.85	0.64	13.31 (12.32)
33	0.88	24.67	0.65	14.02 (13.55)

Table S12. Photovoltaic performances of PTQ10:MYBO-based OSCs processed from Eu with different thickness.

Concentration [mg mL^{-1}]	Spin-coating Speed [rpm]	V_{OC} [V]	J_{SC} [mA cm^{-2}]	FF	PCE$_{max}$ (PCE$_{avg}$) [%]	Thickness [nm]
30	1500	0.87	24.86	0.55	11.84 (11.09)	149 ± 2
	2500	0.87	25.24	0.60	13.18 (12.63)	130 ± 6
	4000	0.88	24.67	0.65	14.02 (13.55)	105 ± 1
	6000	0.88	20.72	0.66	12.04 (11.36)	87 ± 4

Table S13. Photovoltaic performances of PTQ10:MYBO-based OSCs processed from Eu with different thermal annealing temperature and time.

Temperature and Time	V_{OC} [V]	J_{SC} [mA cm^{-2}]	FF	PCE$_{max}$ (PCE$_{avg}$) [%]
140°C 5 min	0.90	20.34	0.68	12.48 (12.08)
120°C 5 min	0.89	22.82	0.68	13.74 (13.28)
100°C 5 min	0.89	24.39	0.68	14.79 (14.23)
100°C 10 min	0.88	25.23	0.69	15.14 (14.71)

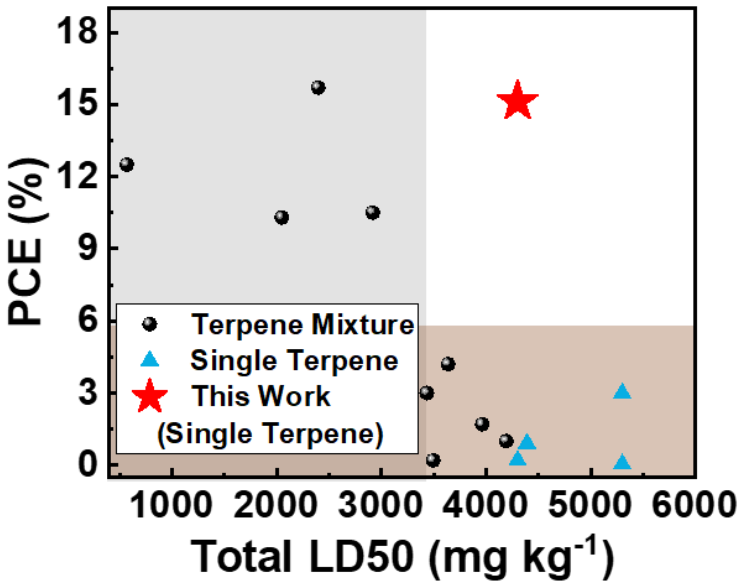

Fig. S9. Summary of PCEs of terpene-based OSCs depending on the total LD50 value from the literature and this work. Total LD50 was calculated by summation of the ATE value.[4]

Table S14. Comparison of the PCE values of the reported terpene-based OSCs (single terpene (Single), terpene + additive (Additive) and terpene mixtures (Mixture)) and this work.

System	Solvent Type	Solvent	Volume Ratio	PCE_{max} [%]	Ref.
PTQ10:MYBO	**Single**	**Eu**	**100**	**15.14**	**This work**
FTAZ:IT-M	**Single**	Limonene	100	0.05	[6]
PBDTTPD:$PC_{61}BM$	**Single**	Eu	100	0.20	[7]
PTB7:$PC_{71}BM$	**Single**	Terpinolene	100	0.91	[8]
PTzBI-Si:PNDICl	**Single**	Limonene	100	3.00	[9]
PBDTTPD:$PC_{61}BM$	**Mixture**	Eu:benzaldehyde	90:10	0.20	[7]
	Additive	Eu:*p*-anisaldehyde	98:2	1.00	
	Mixture	Eu:1-chloronaphthalene	95:5	1.70	
	Mixture	Eu:benzaldehyde:*p*-anisaldehyde	88:10:2	3.00	
P2F-Si:PNDICl	**Additive**	Limonene:*γ*-valerolactone	99.5:0.5	4.20	[9]
PM6:BTP-eC9	**Mixture**	Menthone:tetralin	55:45	10.30	[10]
	Mixture	Limonene:indan	58:42	10.50	
	Mixture	Eu:tetralin	52:48	15.70	

Table S15. SCLC mobilities for the PTQ10:SMA blend films.

SMA	μ_e[a] [$cm^2\ V^{-1}\ s^{-1}$]	μ_h[a] [$cm^2\ V^{-1}\ s^{-1}$]	μ_e/μ_h
L8-BO (CF)	6.9×10^{-4}	3.5×10^{-4}	1.97
L8-BO (Eu)	4.0×10^{-6}	1.5×10^{-4}	0.03
MYBO (CF)	6.1×10^{-4}	3.7×10^{-4}	1.65
MYBO (Eu)	5.9×10^{-4}	3.6×10^{-4}	1.64

[a]Average values obtained from at least 3 independent devices.

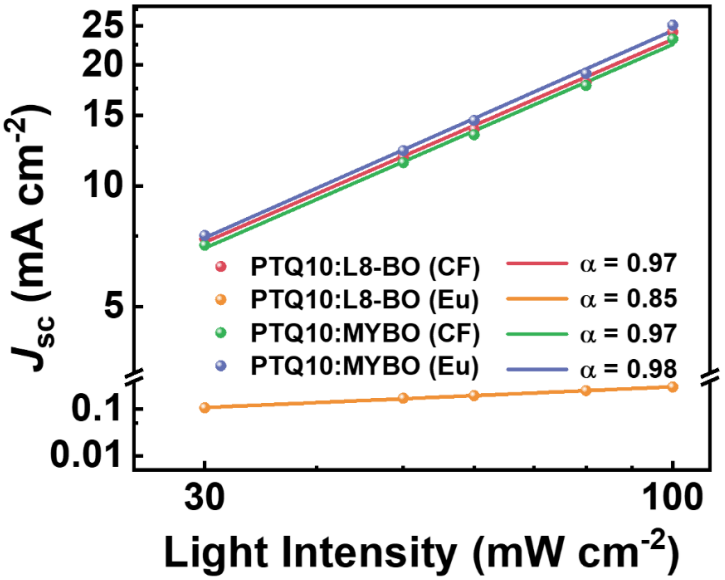

Fig. S10. Light intensity-dependent J_{SC} plots of PTQ10-based OSCs.

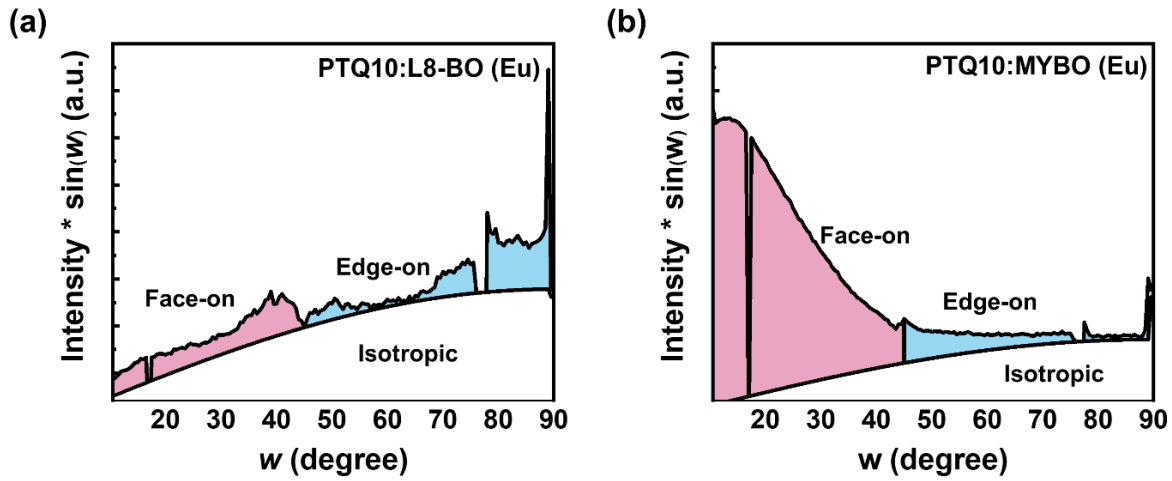

Fig. S11. Orientation of crystalline domains in (a) L8-BO, and (b) MYBO-based blends processed from Eu.

Table S16. Packing orientation of the blends.

	PTQ10:L8-BO (Eu)	PTQ10:MYBO (Eu)
Face-on fraction (%)	8.7	51.3
Edge-on fraction (%)	10.4	5.7
Isotropic fraction (%)	80.9	43.0

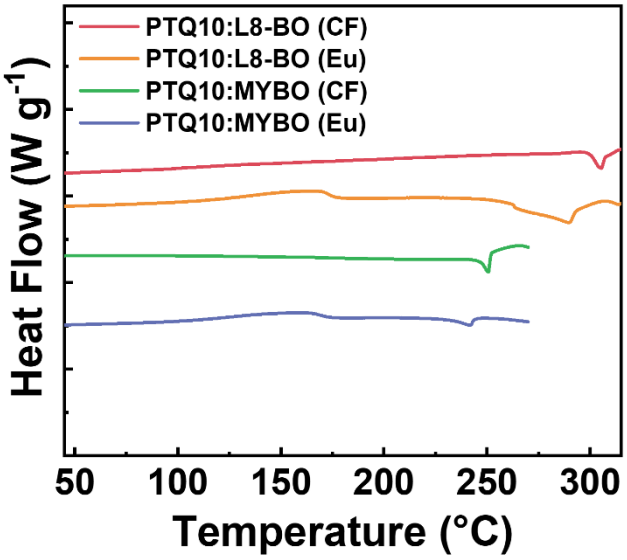

Fig. S12. DSC thermograms of blend films with different processing solvents obtained during the 1st heating cycle.

Table S17. Optical properties and DSC results of blend films.

Active layer (PTQ10-based)	T_m [°C]	ΔH_m [J g^{-1}]
L8-BO (CF)	306	21.3
L8-BO (Eu)	290	48.3
MYBO (CF)	251	7.4
MYBO (Eu)	242	9.8

Table S18. Saturation times of the absorption of the PTQ10:MYBO in Eu with different processing condition.

Concentration [mg mL^{-1}]	Spin-coating Speed [rpm]	τ_{sat}^{PTQ10} [s]	τ_{sat}^{MYBO} [s]	Thickness [nm]
14	**1800**	33.20	33.85	108 ± 1
20	**2500**	29.50	30.90	106 ± 2
30	**4000**	23.70	26.30	105 ± 1

Table S19. Photovoltaic performance of PTQ10:MYBO in Eu.

System	Processing Condition	V_{OC} [V]	J_{SC} [mA cm^{-2}]	FF	PCE_{max} [%]
PTQ10:MYBO (Eu)	**Glove box (N_2)**	0.88	25.23	0.69	15.14
	Ambient	0.88	24.42	0.68	14.66

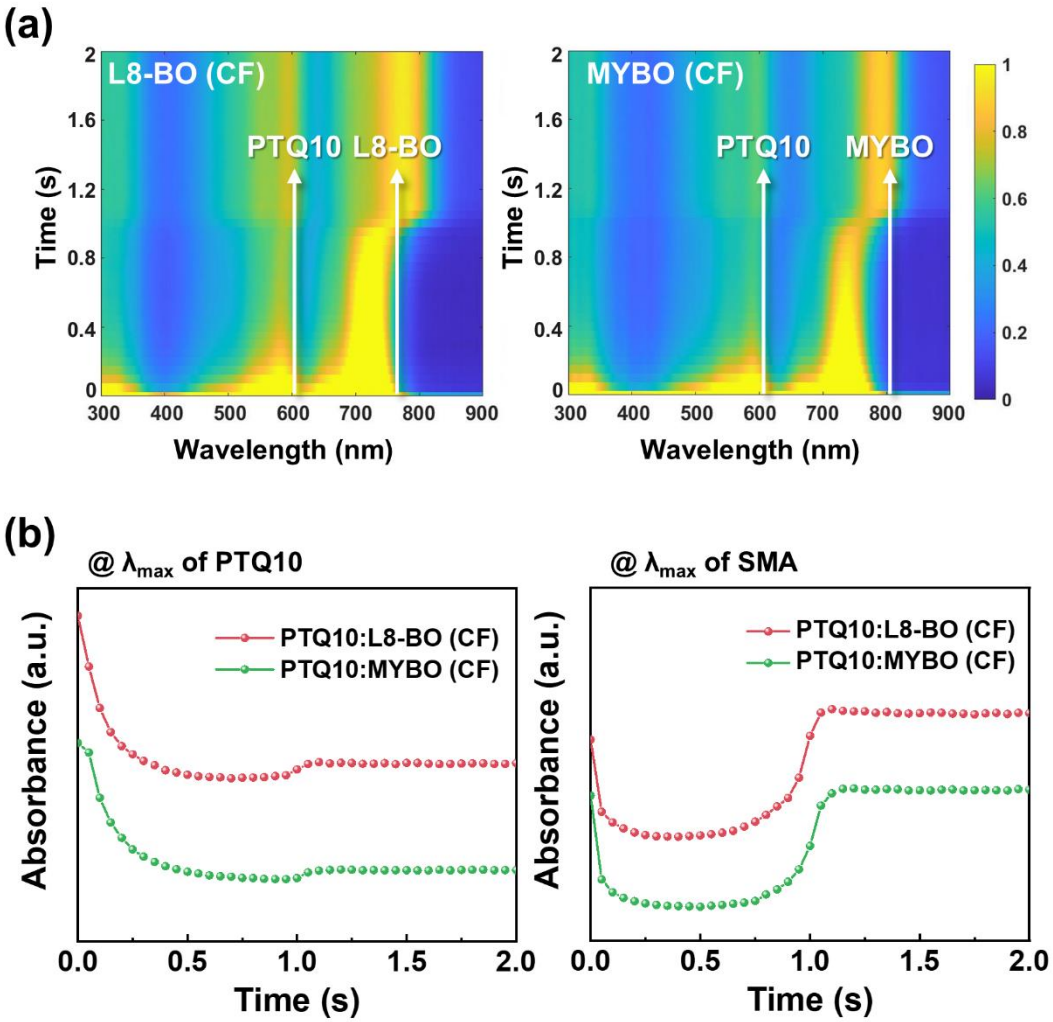

Fig. S13. (a) 2D contour maps of *in-situ* UV–Vis absorption spectra of PTQ10:SMA systems processed with CF and their (b) changes in absorbance at the λ_{max} of PTQ10 and SMA.

Table S20. Saturation times of the absorption of the PTQ10:SMAs in CF.

SMA	τ_{sat}^{PTQ10} [s]	τ_{sat}^{SMA} [s]
L8-BO	1.10	1.10
MYBO	1.15	1.15

References

1. C. Sun, F. Pan, H. Bin, J. Zhang, L. Xue, B. Qiu, Z. Wei, Z.-G. Zhang and Y. Li, *Nat. Commun.*, 2018, **9**, 743.
2. Z. Wu, C. Sun, S. Dong, X.-F. Jiang, S. Wu, H. Wu, H.-L. Yip, F. Huang and Y. Cao, *J. Am. Chem. Soc.*, 2016, **138**, 2004-2013.
3. T. N.-L. Phan, J.-W. Lee, E. S. Oh, S. Lee, C. Lee, T.-S. Kim, S. Li and B. J. Kim, *ACS Appl. Mater. Interfaces*, 2022, **14**, 57070-57081.
4. J. Hamm, D. Allen, P. Ceger, T. Flint, A. Lowit, L. O'Dell, J. Tao and N. Kleinstreuer, *Regul. Toxicol. Pharmacol.*, 2021, **125**, 105007.
5. C. M. Hansen, *Hansen Solubility Parameters: A User's Handbook*, CRC Press, Boca Raton, 2007.
6. L. Ye, Y. Xiong, Z. Chen, Q. Zhang, Z. Fei, R. Henry, M. Heeney, B. T. O'Connor, W. You and H. Ade, *Adv. Mater.*, 2019, **31**, 1808153.
7. C. Sprau, A. M. Cruz, L. Bautista, L. Molina, M. Wagner, C. L. Chochos, M. Della Pirriera and A. Colsmann, *Adv. Energy Sustainability Res.*, 2021, **2**, 2100043.
8. C. Liu, Y. Zhu, J. Chen, H. Wang, Y. Cao and J. Chen, *Synth. Met.*, 2018, **242**, 17-22.
9. M.-J. Li, B.-B. Fan, W.-K. Zhong, Z.-M.-Y. Zeng, J.-K. Xu and L. Ying, *Chin. J. Polym. Sci.*, 2020, **38**, 791-796.
10. D. Corzo, D. Rosas-Villalva, A. C, G. Tostado-Blázquez, E. B. Alexandre, L. H. Hernandez, J. Han, H. Xu, M. Babics, S. De Wolf and D. Baran, *Nat. Energy*, 2023, **8**, 62-73.